July 1991

Angular distribution of electrons following two-photon ionization of the Ar atom and two-photon detachment of the F^- ion

Cheng Pan
University of Nebraska - Lincoln

Anthony F. Starace
University of Nebraska-Lincoln, astarace1@unl.edu

Angular distribution of electrons following two-photon ionization of the Ar atom and two-photon detachment of the F^- ion

Cheng Pan and Anthony F. Starace
Department of Physics and Astronomy, The University of Nebraska, Lincoln, Nebraska 68588-0111
(Received 13 December 1990)

Angular-distribution asymmetry parameters for photoelectrons produced by two-photon ionization of the Ar atom and two-photon detachment of the F^- ion are calculated for photon energies below the thresholds for single-photon ionization and single-photon detachment, respectively. Effects of electron correlations are included by perturbative methods. Good agreement is obtained between our results and those of a recent experimental angular-distribution measurement of two-photon detachment of the F^- ion at $\lambda=532$ nm [C. Blondel, M. Crance, C. Delsart, and A. Giraud (unpublished)].

I. INTRODUCTION

The angular distributions of electrons produced by multiphoton ionization of atoms have been reviewed by Smith and Leuchs [1], particularly for the experimentally important case of resonantly enhanced multiphoton ionization. Such angular distributions not only provide detailed information about resonant intermediate states, but are also sensitive measures of electron-correlation effects [1]. Recently, Blondel *et al.* [2], reported the first experimental measurements of electron angular distributions resulting from the nonresonant multiphoton detachment of negative halogen ions. These measurements were compared with theoretical predictions obtained using a Hartree-Fock (HF) description for the negative halogen ions and a plane-wave description for the detached electrons [2,3]. While these theoretical results agree qualitatively with the experimental measurements [2], there are in general significant quantitative differences that indicate the importance of electron correlations and of detached-electron phase shifts for a more quantitatively accurate theoretical treatment.

In this paper we present detailed theoretical predictions for the angular distributions of photoelectrons produced by two-photon ionization of the Ar atom and two-photon detachment of the F^- ion. Our calculations employ the same treatment of electron correlations in initial, intermediate, and final states as reported by Pan, Gao, and Starace [4] in their calculations of the corresponding total cross sections. Understanding the effects of electron correlations on multiphoton processes is essential for describing the large energy transfers observed experimentally in multiphoton ionization of rare-gas atoms using high-power lasers [5]. While such electron-correlation effects are generally weaker in the isoelectronic negative halogen ions than in the rare-gas atoms, these effects are more simply demonstrated in the negative halogen ions due to the absence of intermediate resonance structures. Furthermore, the lower binding energies of the negative halogen ions have permitted experimentalists to study lower-order multiphoton processes. Finally, absolute experimental cross-section results for the negative halogen ions have recently been obtained [6,7], permitting therefore the most rigorous comparison with theoretical predictions.

In Sec. II we present the theoretical formulas employed in our calculations of the photoelectron angular distribution asymmetry parameters. In Sec. III we present our results for these asymmetry parameters for two-photon ionization of Ar and two-photon detachment of F^-. We also compare our F^- results with the experimental and theoretical results presented in Ref. 2. Finally, in Sec. IV we present our conclusions.

II. THEORY

We are concerned in this paper with the photoelectron angular distributions for the following two processes:

$$\mathrm{Ar}\ 3p^6(^1S)+2\gamma\rightarrow \mathrm{Ar}^+\ 3p^5(^2P)+e^- , \tag{1}$$

$$\mathrm{F}^-\ 2p^6(^1S)+2\gamma\rightarrow \mathrm{F}\ 2p^5(^2P)+e^- . \tag{2}$$

For each of these processes, there are three final-state channels that are important near threshold and which may be described generically as

$$p^6(^1S)+2\gamma\rightarrow p^5(^2P)\epsilon p(^1S) \tag{3}$$

$$\rightarrow p^5(^2P)\epsilon p(^1D) \tag{4}$$

$$\rightarrow p^5(^2P)\epsilon f(^1D) . \tag{5}$$

A. The two-photon transition amplitudes

The exact two-photon transition amplitude from the initial state to one of these asymptotic final states may be written formally as

$$X_{\epsilon l}^{LM}\equiv\left\langle \Psi_{\epsilon l}^-(^1L)\left| D\frac{1}{E_i+\omega-H}D\right|\Psi_i(^1S)\right\rangle . \tag{6}$$

Here H is the exact atomic (ionic) Hamiltonian, E_i is the energy of the initial state, ω is the photon frequency, and D is the electric dipole operator, which in length form is given by

$$D=\hat{\epsilon}_q\cdot\sum_{i=1}^{N}\mathbf{r}_i\ , \tag{7}$$

where $\hat{\epsilon}_q$ is the photon polarization unit vector and $\mathbf{r}_i$ is the coordinate vector of the ith atomic (ionic) electron. [The velocity-form result for the electric dipole operator may be obtained by making the substitution $\mathbf{r}_i\rightarrow -i\mathbf{p}_i/\omega$ in Eq. (7), where $\mathbf{p}_i$ is the momentum operator for the ith electron.] Lastly, $\Psi_i(^1S)$ is the exact initial-state wave function and $\Psi_{\epsilon l}^{-}(^1L)$ is the exact energy-normalized final-state wave function satisfying incoming-wave boundary conditions, as required for photoionization and photodetachment processes [8]. We assume throughout this work that spin-dependent and relativistic interactions may be ignored.

The total cross sections for processes (1) and (2) may be calculated using the transition amplitudes in Eq. (6), in which the final states are represented by the orbital angular momentum l of the photoelectron and its coupling ^1L to the residual atomic (ionic) core. In order to calculate the angular distributions of the photoelectrons, however, we must describe the incoming-wave-normalized final state in terms of the orbital angular-momentum magnetic quantum number M_c of the residual atomic (ionic) core and the relative momentum k of the detached electron. (For simplicity of notation we avoid explicit treatment of the spin magnetic quantum numbers; since the initial states are spin singlets and since we ignore spin-dependent interactions, the treatment of spin is trivial.) Thus, we construct the transition amplitude from the initial state to a final state having core orbital magnetic quantum number M_c and photoelectron momentum k as follows [8]:

$$T_{L_cM_ck}\equiv k^{-1/2}\sum_{l,m}\sum_{L,M}Y_{lm}(\hat{\mathbf{k}})\langle L_cM_clm\,|LM\rangle X_{\epsilon l}^{LM}\ . \tag{8}$$

In Eq. (8), $X_{\epsilon l}^{LM}$ is the transition amplitude defined in Eq. (6) to final states defined by electron energy $\epsilon\equiv k^2/2$, orbital angular momentum l, and total orbital angular momentum LM; the Clebsch-Gordan coefficient projects the final state $|LM\rangle$ onto the uncoupled states $\langle L_cM_clm|$ of the residual atomic (ionic) core (L_cM_c) and the photoelectron (lm), where $L_c=1$ for processes (1) and (2); the spherical harmonic projects the photoelectron state $|lm\rangle$ onto the direction $\hat{\mathbf{k}}$: finally, the prefactor $k^{-1/2}$ is needed to ensure normalization of the final- state wave function defined implicitly by Eq. (8) to a δ function in electron momentum $\mathbf{k}$.

B. Photoelectron angular distributions

The angular distribution of photoelectrons for processes (1) and (2) may be calculated using the following general formula:

$$\sum_{M_c}|T_{L_cM_ck}|^2=k^{-1}\sum_{M_c}\sum_{\substack{l,m,\\ l',m'}}\sum_{\substack{L,M,\\ L',M'}}(X_{\epsilon l'}^{L'M'})^{\dagger}\langle L'M'|L_cM_cl'm'\rangle Y_{l'm'}^{*}(\hat{\mathbf{k}})Y_{lm}(\hat{\mathbf{k}})\langle L_cM_clm\,|LM\rangle X_{\epsilon l}^{LM}\ . \tag{9}$$

Using well-known relations for expressing the product of spherical harmonics as an expansion in single spherical harmonics [9], summing over the magnetic quantum numbers m, m', and M_c using a well-known relation for $3j$ symbols [10], and noting that for the spherically symmetric initial states with which we are concerned here, $M=M'$ is fixed by the polarization q of the incident light, we obtain

$$\sum_{M_c}|T_{L_cM_ck}|^2=(4\pi k)^{-1}\sum_{l,l'}\sum_{L,L'}(X_{\epsilon l'}^{L'M'})^{\dagger}X_{\epsilon l}^{LM}(-1)^{L-M+l}\sum_{\lambda}[\lambda]([l][l'][L][L'])^{1/2}\begin{bmatrix}\lambda & l & l'\\ 0 & 0 & 0\end{bmatrix}\begin{bmatrix}\lambda & L & L'\\ 0 & -M & M\end{bmatrix}$$
$$\times\begin{Bmatrix}\lambda & L & L'\\ L_c & l' & l\end{Bmatrix}P_{\lambda}(\cos\theta_{\hat{\mathbf{k}}})\ . \tag{10}$$

In Eq. (10), $[x]\equiv 2x+1$, $L_c\equiv 1$, P_λ is a Legendre polynomial, $\theta_{\hat{\mathbf{k}}}$ is measured with respect to the axis of linear polarization in the case of linearly polarized incident light and with respect to the incident light beam in the case of circularly polarized light.

The differential cross sections for processes (1) and (2) are given by

$$\frac{d\sigma}{d\Omega}=8\pi^3\alpha^2\omega^2k\sum_{M_c}|T_{L_cM_c\mathbf{k}}|^2\ , \tag{11}$$

which, using Eq. (10), may be written as

$$\frac{d\sigma}{d\Omega}=\frac{\sigma}{4\pi}\sum_{j=0}^{2}\beta_{2j}P_{2j}(\cos\theta_{\hat{\mathbf{k}}})\ . \tag{12}$$

For the case of linearly polarized incident light, the total cross section σ and the asymmetry parameters β_{2j} $(j=0,1,2)$ are defined in terms of the two-photon transition amplitudes $X_{\epsilon l}^{LM}$ in Eq. (6) as follows:

$$\sigma=8\pi^3\alpha^2\omega^2(|X_{\epsilon p}^{00}|^2+|X_{\epsilon p}^{20}|^2+|X_{\epsilon f}^{20}|^2)\ , \tag{13}$$

$$\beta_0=1\ , \tag{14}$$

$$\beta_2=\frac{8\pi^3\alpha^2\omega^2}{\sigma_{2p}}\{|X_{\epsilon p}^{20}|^2+\tfrac{8}{7}|X_{\epsilon f}^{20}|^2 +2\,\mathrm{Re}[-2^{1/2}X_{\epsilon p}^{00\dagger}X_{\epsilon p}^{20}+X_{\epsilon p}^{00\dagger}X_{\epsilon f}^{20} -(6^{1/2}/7)X_{\epsilon p}^{20\dagger}X_{\epsilon f}^{20}]\}\ , \tag{15}$$

$$\beta_4=\frac{8\pi^3\alpha^2\omega^2}{\sigma_{2p}}[\tfrac{6}{7}|X_{\epsilon f}^{20}|^2-(6^{3/2}/7)2\,\mathrm{Re}(X_{\epsilon p}^{20\dagger}X_{\epsilon f}^{20})]\ . \tag{16}$$

For the case of circularly polarized incident light, the corresponding partial cross sections and asymmetry parameters are given by

$$\sigma=8\pi^3\alpha^2\omega^2(|X_{\epsilon p}^{22}|^2+|X_{\epsilon f}^{22}|^2)\ , \tag{17}$$

$$\beta_0=1\ , \tag{18}$$

$$\beta_2=\frac{8\pi^3\alpha^2\omega^2}{\sigma_{2p}}[-|X_{\epsilon p}^{22}|^2-\tfrac{8}{7}|X_{\epsilon f}^{22}|^2 +(6^{1/2}/7)2\,\mathrm{Re}(X_{\epsilon p}^{22\dagger}X_{\epsilon f}^{22})]\ , \tag{19}$$

$$\beta_4=\frac{8\pi^3\alpha^2\omega^2}{\sigma_{2p}}[\tfrac{1}{7}|X_{\epsilon f}^{22}|^2-(6^{1/2}/7)2\,\mathrm{Re}(X_{\epsilon p}^{22\dagger}X_{\epsilon f}^{22})]\ . \tag{20}$$

In the above equations, $\mathrm{Re}(a)$ denotes the real part of the complex number a.

C. Treatment of electron correlations

Our treatment of electron-correlation effects in initial, intermediate, and final states when calculating the two-photon transition amplitudes in Eq. (6) has been described in great detail in Ref. [4]. Briefly, we replace the exact Hamiltonian H by the sum

$$H=H_{\mathrm{HF}}+V\ , \tag{21}$$

where H_{HF} is an LS-dependent Hartree-Fock (HF) potential and V is defined by

$$V\equiv\sum_{\substack{i,j\\ i>j}}\frac{1}{r_{ij}}-V_{\mathrm{HF}}\ . \tag{22}$$

Within a frozen-core approximation, the initial and final states as well as the transition operator in Eq. (6) are expanded in powers of V. The result is that the transition amplitude in Eq. (6) is expressed as a sum of terms, the lowest-order one representing the HF result for the transition amplitude, and the higher-order terms representing electron-correlation effects in the initial, intermediate, and final states. We have treated intermediate-state interchannel interactions to infinite order in V; all other electron correlations have been treated to first order in V, except that interchannel interactions between the final $l=1$ and 3 states have been ignored. Finally, the incoming-wave boundary condition on the final-state wave function in Eq. (6) is applied with respect to spherical waves in the case of F^- and with respect to Coulomb spherical waves in the case of Ar.

Specifically, the exact amplitude $X_{\epsilon l}^{LM}$ in Eq. (6) is approximated in this paper by

$$X_{\epsilon l}^{LM}=i^{-l}\exp(-i\sigma_l-i\delta_l)3^{-1/2}\begin{bmatrix}L & 1 & 1\\ M & -q & -q\end{bmatrix}T_{i\to f}\ . \tag{23}$$

In Eq. (23), the phase factor $i^{-l}\exp(-i\sigma_l-i\delta_l)$ is needed to satisfy the incoming-wave boundary condition, where

$$\sigma_l=\arg\Gamma[l+1-i(Z-N)/k] \tag{24}$$

is the usual Coulomb phase (where Z is the charge of the nucleus and N is the number of electrons on the residual atomic or ionic core), and where δ_l is the LS-dependent HF phase shift with respect to a Coulomb spherical wave in the case of Ar and with respect to a spherical wave in the case of F^-. The factor $3^{-1/2}$ times the $3j$ coefficient in Eq. (23) gives the magnetic quantum number dependence of the transition amplitude, where q is 0 for linearly polarized light and q is 1 for right circularly polarized light. (The square of this factor is denoted by f_q in Eq. (53) of Ref. [4].) Finally, the amplitude $T_{i\to f}$ denotes the sum of amplitudes enumerated in Table I of Ref. [4] and discussed in detail in Sec. II of Ref. [4].

III. RESULTS

A. Two-photon ionization of argon

Our results for the angular distribution asymmetry parameters β_2 and β_4 for process (1) are given in Fig. 1 in the case of linearly polarized light and in Fig. 2 in the case of circularly polarized light. [Note that Fig. 2 only presents β_4; β_2 equals $-\beta_4-1$ in the case of circularly polarized light, as may be verified by an examination of Eqs. (17), (19), and (20).] All three channels in Eqs. (3)–(5) contribute in the case of linearly polarized light, whereas only the ^1D channels contribute in the case of circularly polarized light. As was found in Ref. [4], electron-correlation effects are most significant for the ^1S final-state channel. This explains the much larger discrepancy between the HF length and velocity results for the case of linearly polarized light than for the case of circularly polarized light.

The resonance structures clearly evident in Figs. 1 and 2 are due to intermediate states. Just below $\hbar\omega\approx 12$ eV is the Ar $3p^5 4s(^1P)$ state; just above $\hbar\omega\approx 14$ eV are the Ar $3p^5 3d(^1P)$ and Ar $3p^5 5s(^1P)$ states; and near $\hbar\omega\approx 15$ eV are the Ar $3p^5 4d(^1P)$ and Ar $3p^5 6s(^1P)$ states, which are unresolved in our figures. Although these resonances introduce major discrepancies between the HF level length and velocity results, agreement of our correlated length and velocity results is substantially better. The variational procedures [11] applied in Ref. [4] to the calculation of each contribution to the correlated transition amplitude have also played a significant role in obtaining reliable numerical results even near intermediate-state resonances.

Moccia, Rahman, and Rizzo [12] have also calculated the angular distributions for two-photon ionization of argon. However, they do not present data on the angular-distribution asymmetry parameters, but instead plot the differential cross section as a function of angle. Their re-

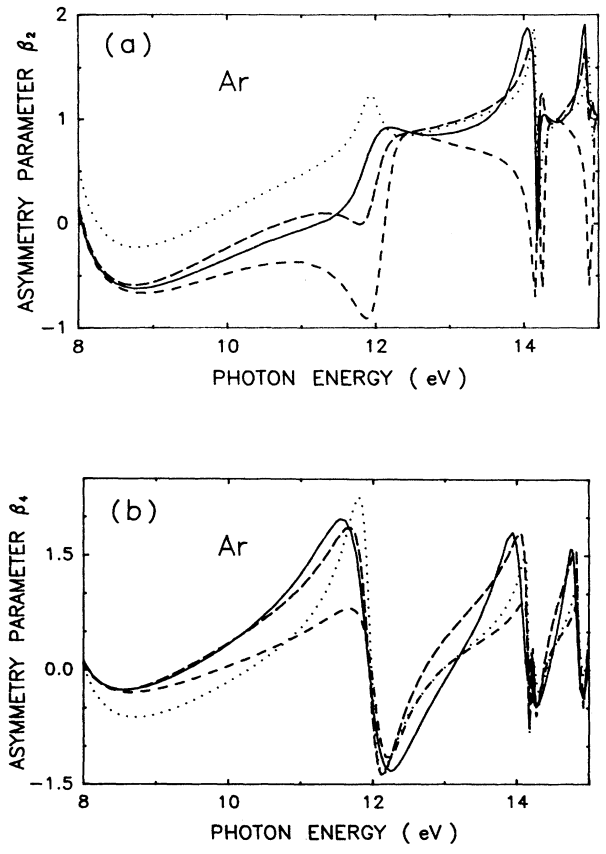

FIG. 1. Photoelectron angular-distribution asymmetry parameters β_2 and β_4 for the process $Ar+2\gamma \rightarrow Ar^+ + e^-$ for the case of linearly polarized light. Short-dashed curves: present HF length results. Dotted curves: present HF velocity results. Solid curves: present correlated length results. Long-dashed curves: present correlated velocity results.

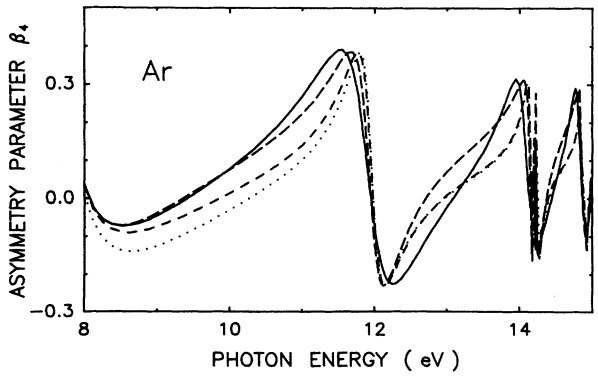

FIG. 2. Photoelectron angular-distribution asymmetry parameter β_4 for the process $Ar+2\gamma \rightarrow Ar^+ + e^-$ for the case of circularly polarized light. Curves are identified as in Fig. 1. Note that for circularly polarized light, $\beta_2 = -1-\beta_4$.

sults, obtained using a simplified random-phase approximation, show substantial discrepancies between length and velocity results, particularly for photoelectrons ionized near $\theta = 0°$. We note also that their total cross sections in dipole length approximation were shown in Ref. [4] to be substantially larger than the total cross sections obtained using the transition amplitudes employed in the present work [13].

B. Two-photon detachment of F^-

Many of the comments given for our asymmetry parameter results for Ar apply also to our asymmetry parameter results for F^-, which are given in Figs. 3 and 4. In particular, since the ^1S channel only contributes in the case of linearly polarized light, electron-correlation effects, which are most significant for this channel, are also most evident in F^- for the case of linearly polarized light. Also, only β_4 is given for the case of circularly polarized light since $\beta_2 = -\beta_4 - 1$, as discussed above. In all cases, our correlated length and velocity results are in quite good agreement, which is in contrast to our HF lev-

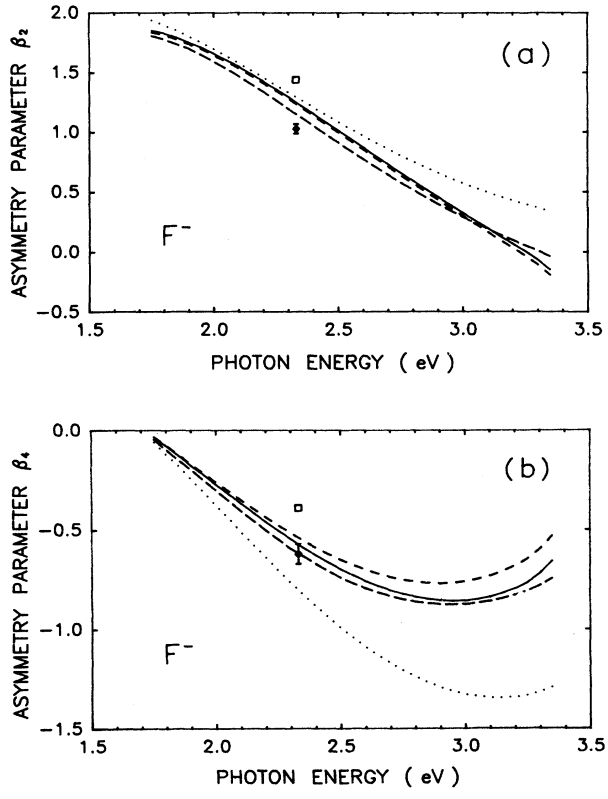

FIG. 3. Photoelectron angular distribution asymmetry parameters β_2 and β_4 for the process $F^- + 2\gamma \rightarrow F + e^-$ for the case of linearly polarized light. Curves are identified as in Fig. 1. Solid diamonds: experimental results of Blondel *et al.* [Ref. [2(b)]]. Open squares: free-electron model theoretical results of Crance [Refs. [2(b)] and [3]].

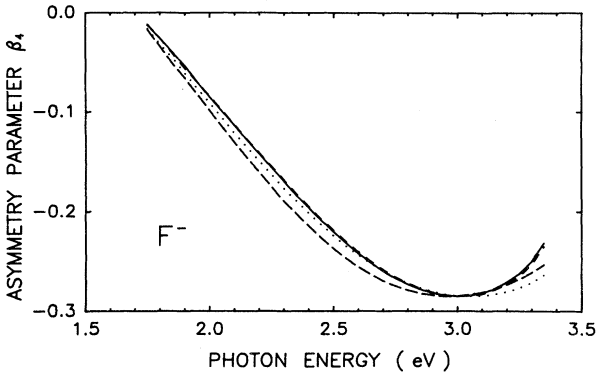

FIG. 4. Photoelectron angular-distribution asymmetry parameter β_4 for the process $F^- + 2\gamma \rightarrow F + e^-$ for the case of circularly polarized light. Curves are identified as in Fig. 1. Note that for circularly polarized light, $\beta_2 = -1 - \beta_4$.

el length and velocity results, particularly for the case of linear polarization.

Figure 3 shows also the experimentally measured results of Blondel *et al.* [2(b)] at $\lambda = 532$ nm as well as the results of a theoretical calculation [2(b), 3] in which the detached electron is treated as a free electron. For both β_2 and β_4 the free-electron calculation [2(b), 3] results lie significantly above the experimentally measured results. For β_2, our correlated length and velocity results lie closer to the experimental results, but above it. For β_4, however, our correlated length and velocity results both pass through the error bars of the experimental result.

Comparison of the different theoretical results for the differential cross section with a typical set of relative experimental results at $\lambda = 532$ nm is given in Fig. 5. In Fig. 5(a) we plot results for the normalized angular distribution [cf. Eq. (12)]:

$$4\pi\sigma^{-1}\frac{d\sigma}{d\Omega} = 1 + \beta_2 P_2(\cos\theta_{\hat{k}}) + \beta_4 P_4(\cos\theta_{\hat{k}}) \ . \qquad (25)$$

Such a plot pinpoints the angular region in which the differences in the measured and calculated values for β_2 and β_4 shown in Fig. 3 can be most easily observed. For this plot the relative experimental points have been fit (using a least-squares procedure) to our correlated results for the right-hand side of Eq. (25), which are nearly indistinguishable from our corresponding HF results at this wavelength. This near agreement has two causes: first, our use of HF final-state phase shifts, and second, the fact that the asymmetry parameters are ratios of transition amplitudes and that the differences in the magnitudes of the transition amplitudes are not so prominent in the ratios at this wavelength. The quite good agreement of our curves with the experimental results indicates that for this light ion the HF phase shifts represent a reasonable approximation. The remaining discrepancies, primarily near 0° and 180°, most likely indicate the necessity for theory to improve the predictions for the final-state phase shifts. At 0° and 180° the discrepancies of the experimental results with the theoretical calculations [2(b), 3] employing a free-electron description for the final state is pronounced, indicating clearly the importance of a proper description of the final-state phase shifts. It should be emphasized that the relative experimental measurements have been fit to our correlated results and not to the results of the free-electron calculation shown in Fig. 5(a). To this extent the free-electron results are shown at a disadvantage. Statistical measures, however, show that this disadvantage is not severe [14], and for this reason we have opted to present all of the results in Fig. 5(a) in a single figure rather than in separate figures.

Figure 5(b) compares our theoretical results for the differential cross section $d\sigma/d\Omega$ at $\lambda = 532$ nm with the relative experimental measurements, which have been normalized to our correlated results by a least-squares procedure. Our results in Fig. 5(b) are obtained by multi-

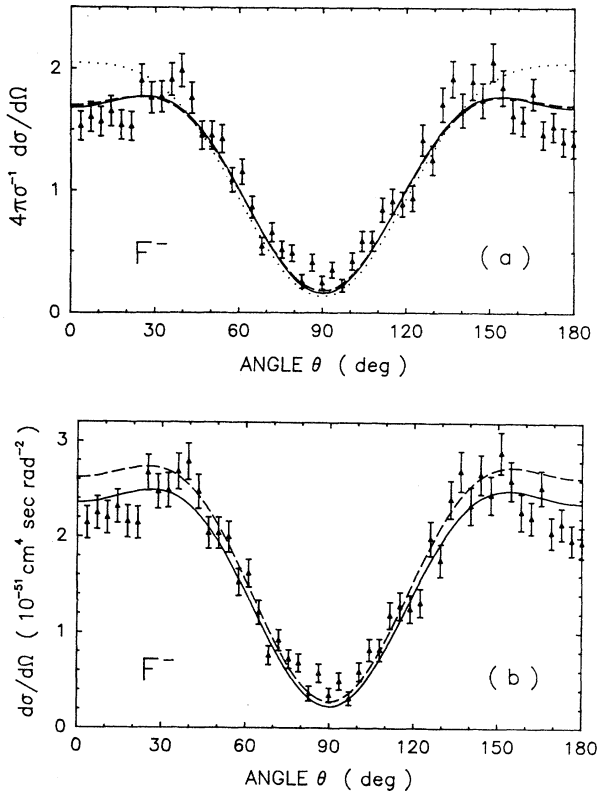

FIG. 5. Differential cross sections for the process $F^- + 2\gamma \rightarrow F + e^-$ for the case of linearly polarized light and $\lambda = 532$ nm. (a) Normalized differential cross section, $4\pi\sigma^{-1}d\sigma/d\Omega$. (b) Differential cross section, $d\sigma/d\Omega$. Solid curves: present correlated length results. Dashed curves: present HF length results. Dotted curve [in (a) only]: free-electron length results of Crance [Refs. [2(b)] and [3]]. Solid triangles: relative experimental results of Blondel *et al.* [Ref. [2(b)]]. The relative experimental results have been normalized in this figure to our correlated length results using a least-squares-fitting procedure.

plying those in Fig. 5(a) by $\sigma/4\pi$. Now our HF and correlated results differ significantly, most prominently at 0° and 180° where the differential cross section is largest, due to the differences in our results for the total cross section at this wavelength. The free-electron results [2(b), 3] are not shown in this figure since they lie a factor of 2 higher than ours, as has been shown already in Fig. 11 of Ref. [4].

IV. CONCLUSIONS

In this paper we have presented detailed theoretical calculations for the photoelectron angular distributions resulting from two-photon ionization of Ar and two-photon detachment of F^-. These results present a further test for the theoretical approach presented by Pan, Gao, and Starace [4]. For Ar, our treatment of electron correlations is shown to be sufficiently good that length and velocity results for the asymmetry parameters are in reasonable agreement, even in the neighborhood of intermediate-state resonance features. Our use of variational techniques to calculate the transition-matrix elements is an important element in obtaining this good agreement, as is, of course, our selection of which electron-correlation effects to include.

For F^- our correlated results have been shown to give reasonable agreement with the experimentally measured results of Blondel *et al.* [2(b)]. Comparisons of our correlated results with our HF results as well as with the free-electron calculations of Crance [[2(b)] and [3]] indicate that for F^- the experimental results present a sensitive test for theoretical approximation methods, especially near 0° and 180°. In particular, proper theoretical treatment of the photodetached electron's phase shift has been shown to be essential for the theoretical description of the experimental results near 0° and 180°.

ACKNOWLEDGMENTS

One of us (A.F.S.) gratefully acknowledges discussions and correspondence with C. Blondel and M. Crance regarding their experimental and theoretical work and thanks them for providing their angular distribution asymmetry parameter results for F^- prior to publication. This work was supported in part by National Science Foundation Grant No. PHY-8908605.

[1] S. J. Smith and G. Leuchs, Adv. At. Mol. Phys. **24**, 157 (1987).

[2] (a) For Br^-, see C. Blondel, M. Crance, C. Delsart, A. Giraud, and R. Trainham, J. Phys. B **23**, L685 (1990); (b) For F^-, see C. Blondel, M. Crance, C. Delsart, and A. Giraud (unpublished).

[3] M. Crance, J. Phys. B **21**, 3559 (1988).

[4] C. Pan, B. Gao, and A. F. Starace, Phys. Rev. A **41**, 6271 (1990).

[5] A. L'Huillier, L. A. Lompré, G. Mainfray, and C. Manus, Phys. Rev. Lett. **48**, 1814 (1982); T. S. Luk, H. Pummer, K. Boyer, M. Shahidi, H. Eggar, and C. K. Rhodes, Phys. Rev. Lett. **51**, 110 (1983). See also the introductory section of Ref. [4] and Refs. [1]–[27] quoted therein concerning other experimental and theoretical work on multiphoton ionization of rare-gas atoms and multiphoton detachment of their isoelectronic negative ions.

[6] C. Blondel, R.-J. Champeau, M. Crance, A. Crubellier, C. Delsart, and D. Marinescu, J. Phys. B **22**, 1335 (1989).

[7] N. Kwon, P. S. Armstrong, T. Olsson, R. Trainham, and D. J. Larson, Phys. Rev. A **40**, 676 (1989).

[8] See, e.g., A. F. Starace, in *Corpuscles and Radiation in Matter I,* Vol. 31 of *Handbuch der Physik,* edited by W. Mehlhorn (Springer, Berlin, 1982), Sec. 4.

[9] A. R. Edmonds, *Angular Momentum in Quantum Mechanics,* 2nd ed. (Princeton University Press, Princeton, NJ, 1974), Eq. (4.6.5).

[10] A. P. Yutsis, I. B. Levinson, and V. V. Vanagas, *Theory of Angular Momentum* (Israel Program for Scientific Translations, Jerusalem, 1962), Eq. (A.7.4).

[11] B. Gao and A. F. Starace, Phys. Rev. Lett. **61**, 404 (1988); Phys. Rev. A **39**, 4550 (1989).

[12] R. Moccia, N. K. Rahman, and A. Rizzo, J. Phys. B **16**, 2737 (1983), Fig. 8.

[13] Cf. Fig. 6 of Ref. [4].

[14] The experimental data shown in Fig. 5 have been normalized to our correlated length results by a least-squares fit giving $\chi^2=2.46$. When the data so fit are compared with the free-electron results shown in Fig. 5(a), one obtains $\chi^2=6.90$. If these experimental results are normalized instead to the free-electron results using a least-squares fit, one obtains an improvement of χ^2 to the value of 5.84.